Bridge monitoring using six-component ground motion measurements

Shihao Yuan*[1], Felix Bernauer[2], Chun-Man Liao[3], Ernst Niederleithinger[3], Eileen R. Martin[1,5], Céline Hadziioannou[4], Joachim Wassermann[2], and Heiner Igel[2]

[1]Department of Geophysics, Colorado School of Mines

[2]Department of Earth and Environment Sciences, Ludwig-Maximilians-Universität München

[3]Bundesanstalt für Materialforschung und -prüfung

[4]Institute of Geophysics, University of Hamburg, Germany

[5]Department of Applied Math and Statistics, Colorado School of Mines

October 13, 2024

Key words: Structural health monitoring (SHM), Bridge monitoring, Rotation measurements, Inclinometers, Rotational sensors, Bridge damage detection, Non-destructive testing, Modal analysis

*E-mail: syuan@mines.edu

Abstract

In the context of ageing infrastructure, structural health monitoring is crucial for safety and integrity assessment, as well as for planning preventive maintenance. While classical methods rely on single-component sensors to track vibrations and identify structural changes, this paper proposes an alternative approach for real-time, continuous seismic structural health monitoring. Our system uses collocated triaxial seismometers and rotational sensors (six-component or 6C measurements). In a validation experiment, we simulate damage through controlled loading and prestressing with weight-drop sources generating elastic waves on a concrete bridge model. This study demonstrates the effectiveness and high spatiotemporal resolution of the proposed amplitude-ratio method using 6C data for monitoring structural changes. The approach is further validated through traditional modal analysis and numerical simulations.

1 Introduction

Bridges are essential components of our transportation infrastructure. Their structural integrity ensures public safety and economic stability. However, bridges can deteriorate over time due to factors such as corrosion, fatigue, environmental conditions, and natural hazards. This damage can become severe and threaten bridge safety. According to a 2021 report by the American Society of Civil Engineers, over 42,000 bridges in the United States are considered structurally deficient (InfrastructureCard, 2021). Similarly, many bridges worldwide are also surpassing their intended service lives. Many bridges around the world are exceeding their intended service lives and may sustain undetected structural damage from earthquakes and storms, which further reduces their lifespan and deteriorates their condition. Replacing all deficient bridges is cost-prohibitive, so it is essential to accurately identify which bridges are safe for use and which require repair, reinforcement, or replacement.

Seismic Structural Health Monitoring (S^2HM) is a powerful tool that can offer invaluable insights into bridge behavior and safety (Limongelli and Çelebi, 2019). Traditional S^2HM methods have primarily relied on sensors like geophones to monitor vibrations, resonance frequencies, modal shapes, and other parameters. These measurements provide insights into the structural behavior of bridges over time and across different locations, allowing for the identification of potential weaknesses or damage. However, current methods often face challenges such as limited ability to frequently repeat measurements, insufficient spatial coverage, and the need for extensive sensor installation, which can be time-consuming, costly, and disruptive to bridge traffic.

In recent years, there has been a growing interest in developing S^2HM techniques that can offer real-time, continuous monitoring capabilities. One emerging approach is the use of rotational seismic measurements. Traditional seismic monitoring usually depends on instruments like accelerometers, seismometers, or geophones to measure translational motions, specifically, particle velocities or accelerations. However, these instruments do not fully capture the complex

dynamic behavior of structures. Rotational sensors, also known as inclinometers or tiltmeters, are used to measure how objects are rotated, which is key information for the navigation and stabilization systems of aircraft, spacecraft, and submarines. In seismology, researchers use rotational sensors for various applications (Lee et al., 2009; Sollberger et al., 2020), including seismic source characterization (Donner et al., 2016; Yuan et al., 2021), seismometer tilt correction (Lin et al., 2010; Bernauer et al., 2020b), imaging and monitoring of Earth's structures (Bernauer et al., 2009; Barak et al., 2018; Yuan et al., 2020), planetary surveys (Bernauer et al., 2020a), site response analysis (Wang et al., 2009; Keil et al., 2021).

For S^2HM, Zembaty et al. (2014) analyzed a non-destructive damage detection method that reconstructs changes in structures' stiffness distribution by measuring their rotational response to harmonic vibrations. In bridge monitoring, Alten et al. (2017) evaluated vibration, rotation, and strain data from an instrumented bridge subjected to various damage scenarios. Their findings showed that the rotational sensors provided the most reliable indication of structural damage, outperforming accelerometers, which failed to detect some damage scenarios. Similarly, Hester et al. (2020) and McGeown et al. (2021) used rotation as a damage-sensitive parameter by comparing the rotational influence line of a healthy bridge with that of a damaged one. Experimental validation in the laboratory by Huseynov et al. (2020) further supported these findings. Additionally, Alamdari et al. (2019) used rotation-influence lines as a damage indicator in simulations based on a 3D finite element model calibrated with field data from a bridge.

Obrien et al. (2021) showed that the rotational measurements are more sensitive to local damages than strain measurements based on Bridge Weigh-in-Motion systems. Several studies have extended conventional methods to extract modal properties of bridges using rotation data (Heng et al., 2014). More recently, Rossi et al. (2024) presented an unscented Kalman filter for combining data from accelerometer, GNSS, and rotational sensors to correct rotation-induced errors and accurately track motion on a pedestrian bridge under various excitations.

While rotation-based bridge monitoring techniques have proven valuable for understanding structural behavior, few studies have combined both translational and rotational measurements for bridge damage identification and localization. This gap is likely due to limitations in early sensor technology. Before mid-late 2000s, commercially available, high-accuracy rotational sensors with sampling rates comparable to traditional vibration sensors were not widely available. However, advances in rotational sensors over the past decade have enabled the development of a novel data acquisition system. This system combines triaxial seismometers and rotational sensors, collectively refer to as a six-degree-of-freedom (6DoF) or six-component (6C) measurement system.

The 6C system provides a more comprehensive view of a bridge's dynamic behavior and structural changes, with minimal influence from environmental factors or vibration source parameters. The study has two key objectives: (1) to develop and test a novel and efficient S^2HM technique, and (2) to leverage the unique advantages of 6C measurements.

This approach aims to provide continuous monitoring capabilities, enabling early detection of structural changes and facilitating preventative maintenance. The use of 6C measurements offers the potential for enhanced sensitivity, improved spatial and temporal resolution in damage detection.

We evaluate the proposed approach through controlled experiments on a large-scale concrete bridge model. These experiments simulate varying loading processes, prestress loss and damage scenarios. We generate elastic waves using a weight-drop source. Damage detection and location are then performed based on the 6C vibration data. The results are then validated through numerical modeling and analysis that imitates the real bridge experiment.

2 Theoretical foundations

Severe damage can occur during resonance vibrations, which behave like standing waves. To formulate the simplest single-mode standing wave, we consider two identical transverse waves moving in opposite directions along the x-axis of a bridge:

$$u_{z1}(x,t) = A\sin(kx+\omega t), \quad u_{z2}(x,t) = A\sin(kx-\omega t), \tag{1}$$

where u_{z1} and u_{z2} represent the vertical displacement of the two waves, each with an amplitude A, wavenumber k, and time t. We then add these waves, resulting in the standing wave:

$$u_z(x,t) = u_{z1} + u_{z2} = 2A\sin(kx)\cos(\omega t). \tag{2}$$

Rotational motions (R) are the curl of translational motions. The amplitude ratio (ϕ) between the accelerogram ($\ddot{u}_z$) and rotational rate ($\dot{R}_y$) of the standing wave can be expressed as follows:

$$\phi = \left|\frac{\ddot{u}_z}{\mathscr{H}(\dot{R}_y)}\right| = \left|\frac{\omega}{k}\tan(kx)\right| = v|\tan(kx)|, \tag{3}$$

where $\mathscr{H}$ denotes the Hilbert transform, and v represents the scalar velocity of the propagating waves that form the standing waves. The Hilbert transform is applied to eliminate the 90-degree phase shift between the accelerogram and the rotational rate, allowing for the direct estimation of their amplitude ratios. In a more general scenario, this amplitude ratio will encompass three-component translational recordings (particle displacement, velocity or acceleration) and three-component rotational recordings. Therefore, we refer to this method as the 6C amplitude ratio method. As shown in Equation 3, the amplitude ratio between particle acceleration and rotational rate is directly proportional to the wave velocity and another scaling term, $\tan(kx)$, which is associated with the vibration mode and the position of the 6C receiver.

If we focus on the same single-mode vibration with a fixed 6C receiver, we can treat the scaling term $\tan(kx)$ as a constant value. In the context of Structural Health Monitoring (SHM), where the elastic parameters of the bridges

may vary, changes in relative velocity can be estimated by calculating the relative amplitude variations based on:

$$\frac{dv}{v} = \frac{\phi_1 - \phi_0}{\phi_0}, \tag{4}$$

where ϕ_0 and ϕ_1 represent the 6C amplitude ratio in Equation 3 for baseline and monitoring stages of the bridge, respectively. The relative velocity changes might be an effective indicator of bridges experiencing damages or prestress loss.

3 Real experiments

3.1 Data acquisition and experiment setup

To validate the proposed 6C amplitude-ratio-based measurement, we conduct a real experiment on a 24-meter, two-span bridge model (see Figure 1), which is equipped with an adjustable prestressing system. Two 6C receivers (#1 and #2 in Figure 1) positioned on the two adjacent spans of the bridge, each comprising a co-located seismometer (Trillium Compact 120s) and a rotational sensor (blueSeis-3A). During the experiment, static loads are alternately applied and removed while waves are generated using a weight-drop source at a fixed location. The source, static loads, and the #1 6C receiver are all located on one span, while the #2 6C receiver was situated on the neighboring span.

Some pre-exsisting cracks are visible on the lower surface of the bridge (as shown in Figure 1). The combination of varying prestressing, static loads, and the presence of cracks is expected to influence the elastic properties of the bridge, potentially simulating structural damage or aging. It is worth mentioning that the impact of the horizontally applied prestressing, which affects the entire bridge, differs from the localized perturbations that may result from asymmetric static loads. The two 6C receivers, positioned on each span of the bridge, are intended to evaluate their effectiveness in detecting inhomogeneous structural changes. The localization of structural alterations is further discussed in Section 3.2.

3.2 Real data processing and results

Both prestressing and loading can induce changes in elastic properties of the bridge. Throughout the experiment, we gradually applied a static load, increasing it from 0 to 900 kg in increments of 300 kg for each prestressing conditions. Initially, we extracted the resonance frequencies and analyzed their variations under different loading and prestressing scenarios. Figure 2a illustrates the fundamental resonance frequency (f_0) extracted from vertical acceleration (Acc.Z) recordings, represented by triangles, as a function of time. The corresponding time series are shown in Figure 2c. The retrieved f_0 values under different static loads are distinguished by colors, and each block, separated by dashed

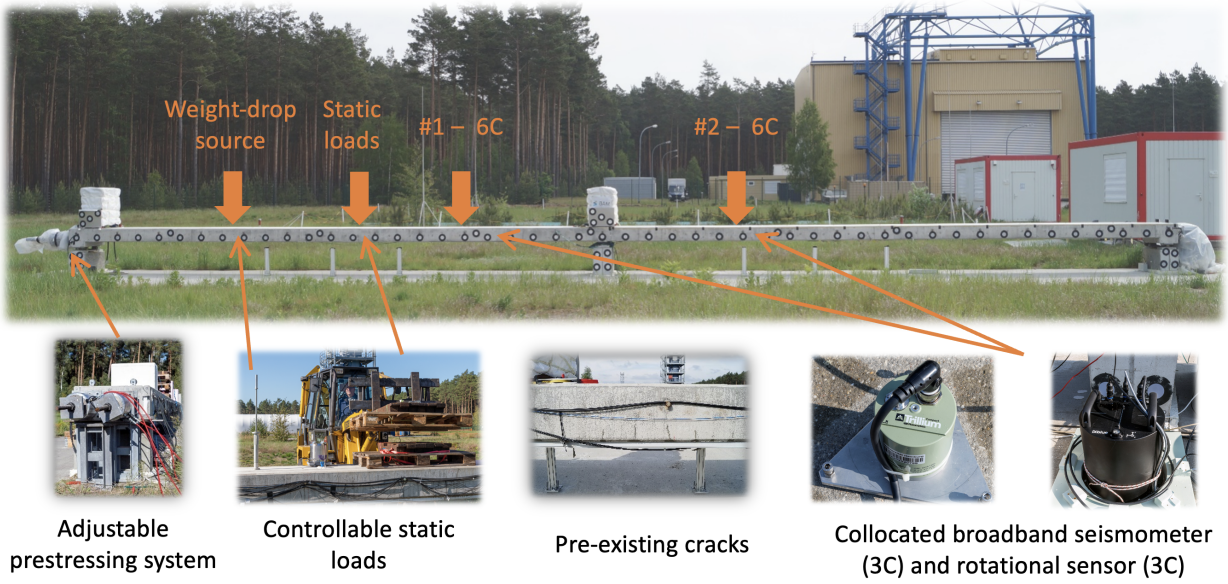

Figure 1: Data acquisition and testing site: The 24-meter two-span bridge model is equipped with an adjustable prestressing system. Two 6C stations (#1 and #2) are deployed, each consisting of a collocated triaxial broadband seismometer (Trillium Compact 120s) and a triaxial rotational sensor (blueSeis-3A) positioned on the two adjacent spans. During the experiment, static loads are applied or removed, and waves are excited using a weight-drop source.

red lines, corresponds to specific prestressing conditions labeled with text numbers. It is observed that the f_0 values decrease as the static load increases. As the static load on a bridge intensifies, the structure's mass increases due to the added weight. Additionally, the static load induces deformation in the structure, which may lead to the opening of pre-existing fractures and result in changes in stiffness.

The total load is increased to 900 kg and then removed when releasing the prestress. Each time, the prestress is reduced by 50 kN, starting from 400 kN, and the loading process is repeated. When comparing the changes in f_0 for the same static load at different prestress levels, we observe a decrease in f_0 as the prestress decreases. As prestress diminishes, the stiffness of the bridge decreases, resulting in a lower resonance frequency. Reduced prestress permits greater deformations under load, affecting the overall stiffness of the structure. Both the increased load and decreased prestress contribute to a reduction in the bridge's resonance frequency. This phenomenon is commonly used to assess and monitor the health of the bridge, especially in extreme cases such as structural failure. The reduction in the retrieved f_0 essentially indicates ongoing structural changes and can be used to validate the proposed 6C method, as detailed below.

We then band-pass filter both translational and rotational recordings, focusing on frequencies between 2 and 4 Hz to capture fundamental mode vibrations. Following this, we apply the 6C amplitude ratio method, as described in Section 2, to estimate the relative velocity changes in the same scenarios analyzed for the resonance frequency. We

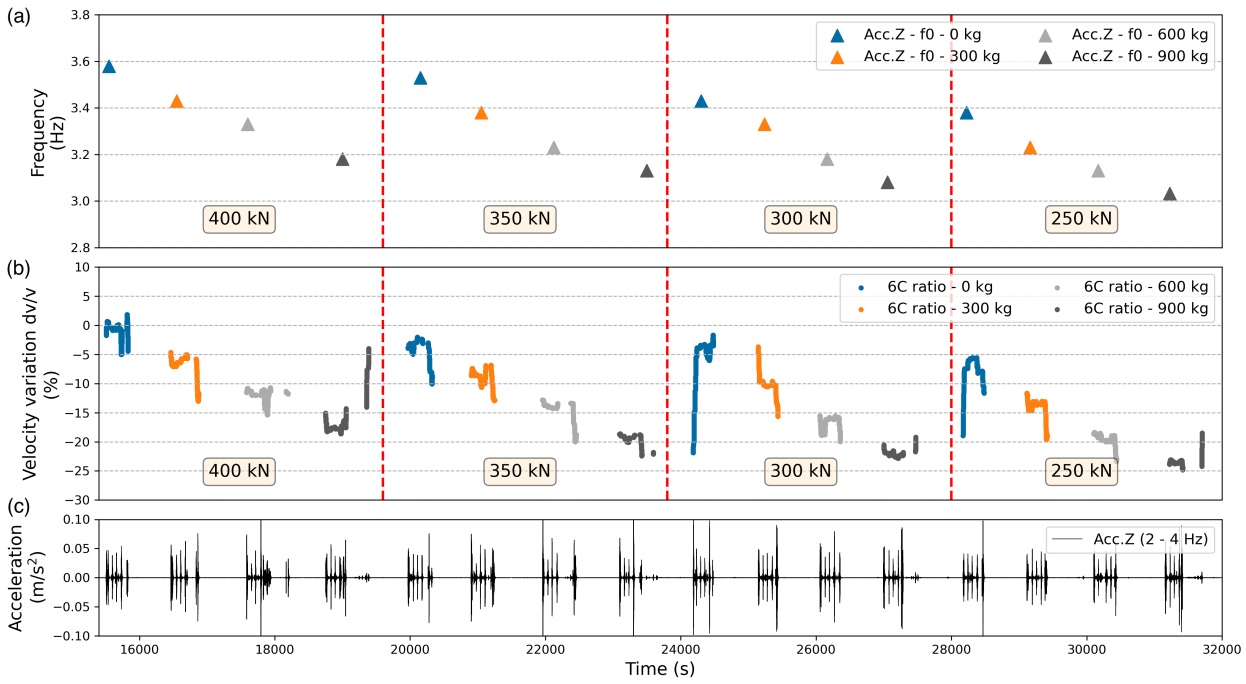

Figure 2: Estimated structural changes based on resonance frequency analysis and the proposed 6C amplitude ratio method. (a) Estimated fundamental resonance frequencies as a function of time. The colors of the triangles are used to differentiate the loading conditions. Each block, separated by dashed red lines, corresponds to specific prestressing conditions labeled with text numbers. (b) Estimated relative velocity changes (dv/v) using the 6C method. The color scheme is consistent with that in (a). (c) Time series of the vertical component of acceleration, band-pass filtered between 2-4 Hz, focusing on fundamental mode vibrations.

consider the estimated amplitude ratio based on Equation 3 under zero static load and 400 kN as our baseline stage. When estimating the amplitude ratios, we employ a sliding window (2 s) and an amplitude threshold (> 5e-5 m/s^2) to exclude estimations derived from signals with poor signal-to-noise ratios. We analyze each sliding window using principal component analysis to calculate the amplitude ratio between translational and rotational motion. In Figures 3–6, each solid dot represents the estimated ratio for a single window. The relative velocity changes, hereinafter referred to as dv/v, when altering static load and prestress, can be calculated using Equation 4. As depicted in Figure 2b, the estimated amplitude ratios in each scenario exhibit consistent behaviors with f_0 in Figure 2a. The relative velocity changes increase as we either increase the static load or decrease the prestress. Some outliers of dv/v can be attributed to the signals when adding load onto the bridge with the forklift rather than the weigh-drop source. This result confirms that the 6C amplitude ratio method is effective in identifying and quantifying structural variations.

When the prestress is raised back from 250 kN to 400 kN, as shown in Figure 3a, the f_0 gradually returns to its initial value. The estimated dv/v, illustrated in Figure 3b, also shows a consistent trend both qualitatively and quantitatively.

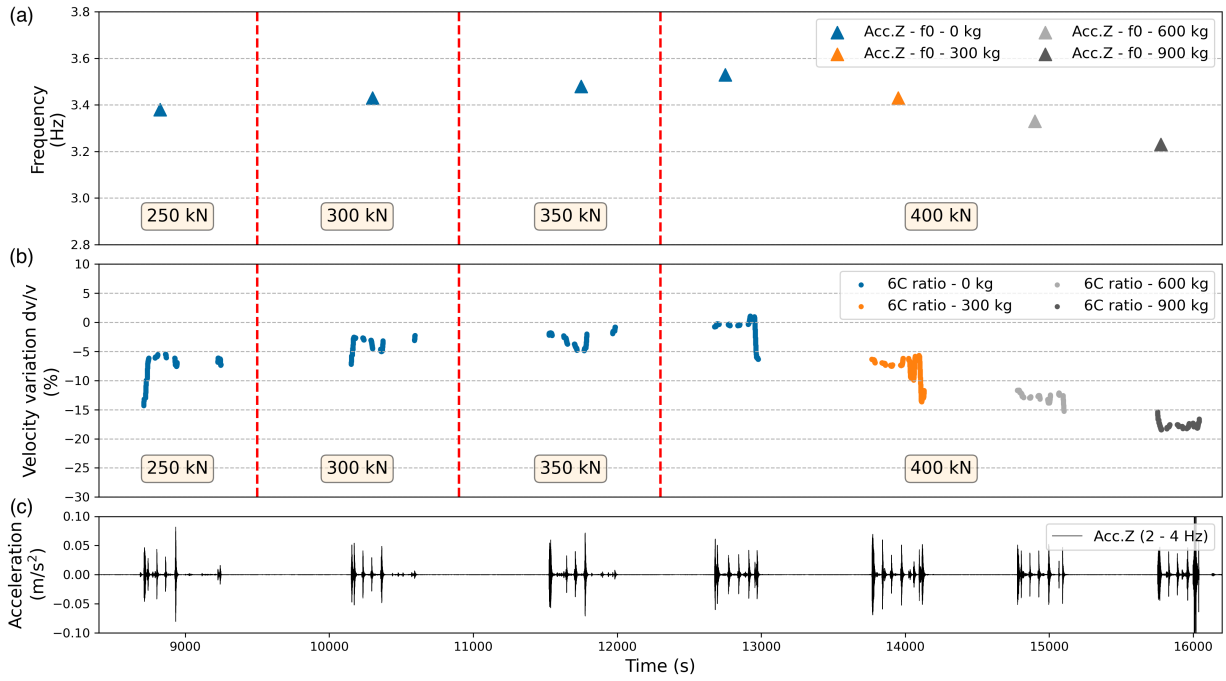

Figure 3: Similar to Figure 2, but for a different loading and prestressing condition.

Upon increasing the static load while maintaining a prestress of 400 kN, both f_0 and dv/v exhibit behavior similar to that observed in Figure 2. This outcome highlights that the reversible structural variations can be accurately detected and quantified by both resonance frequency analysis and the proposed 6C amplitude ratio method.

From the experiments and results discussed above, we demonstrate that the 6C measurement can effectively identify and quantify the structural changes of the bridge. To assess its sensitivity to potential local damage, we examine receivers at each span of the bridge, with one 6C receiver closer to the static load than the other. The static load is expected to induce local structural alterations due to preexisting cracks. We replicate the processing for the #2 6C receiver, and the results are shown in Figure 4. The pattern of the retrieved fundamental resonance frequencies (Figure 4a) at the neighboring span remains nearly the same compared to that in Figure 2a. However, the estimated dv/v at this more distant position (Figure 4b) differs significantly from that obtained near the static load (Figure 2b), although its response to changes in prestress remains consistent at both 6C stations. These differences may be attributed to the distinct effects that prestress and static load introduce to the bridge. Prestress loss tends to induce structural variations uniformly across the entire structure, whereas the static load may prompt more localized changes.

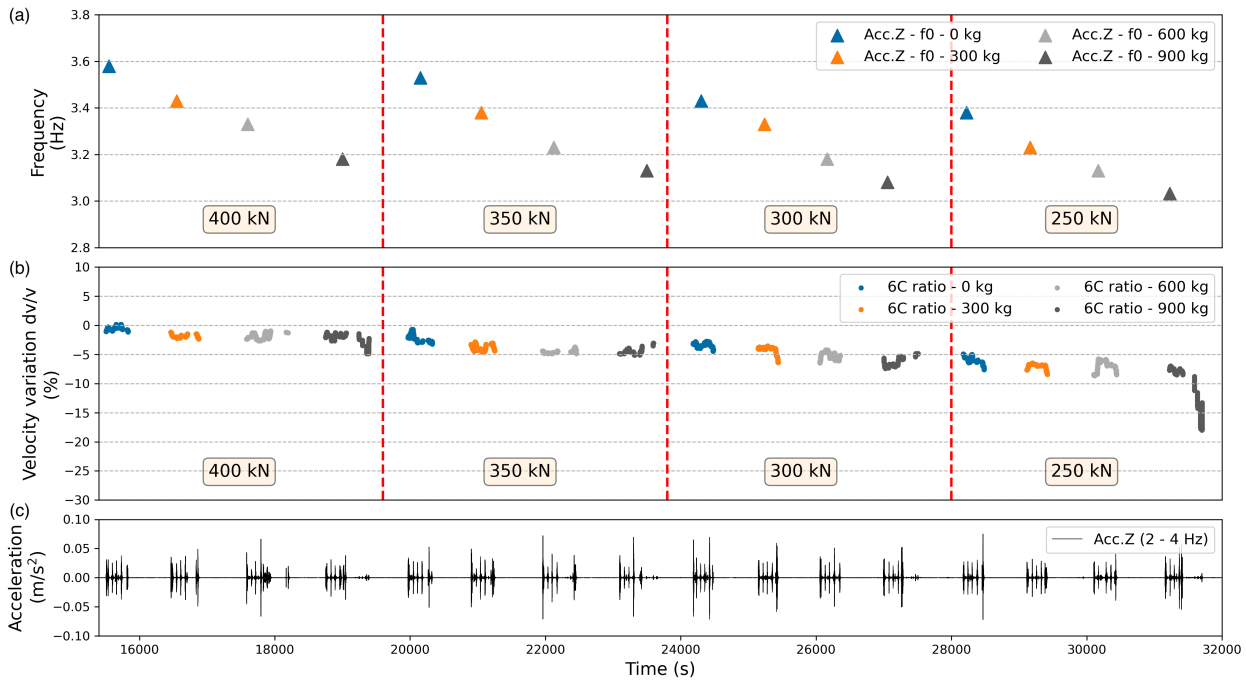

Figure 4: Similar to Figure 2, but for the #2 6C receiver on the neighboring span. In this case, the 6C receiver is positioned on a different span from the source and static loads.

4 Numerical examples

A numerical example is created to simulate the real bridge experiment described in Section 3.1, providing further validation for the proposed 6C amplitude ratio method. As illustrated in Figure 5, the simplified numerical model maintains the same geometry and dimensions with the actual bridge model, while its elastic parameters are detailed in Table 1. Three-dimensional seismic wave propagation simulations along the bridge are performed using SeisSol (https://seissol.readthedocs.io/), an open-source software based on the arbitrary high-order discontinuous Galerkin method (ADER-DG) (Dumbser and Käser, 2006). The bridge model was discretized with an unstructured tetrahedral mesh (Figure 5) using Gmsh (https://gmsh.info/), an open-source mesh generator.

The short-term and long-term structural weakening of the bridge is modeled as a simple reduction in Young's modulus. While this approach is basic, it effectively simulates realistic scenarios, such as the bridge strike incident reported by Pakrashi et al. (2013). As illustrated in Figure 6, we design two sets of numerical tests to validate the proposed 6C method's ability to quantify and locate potential changes in bridge velocity.

In the first set of experiments, we use a single source and a single 6C receiver positioned at fixed locations. We gradually reduce Young's modulus homogeneously four times, each reduction by 2%. We then examine how the measured dv/v changes with the decreasing Young's modulus (Figure 6a). In the second set, we use a single source and a line of 6C receivers. To mimic localized bridge damage, we locally reduce Young's modulus in a specific region

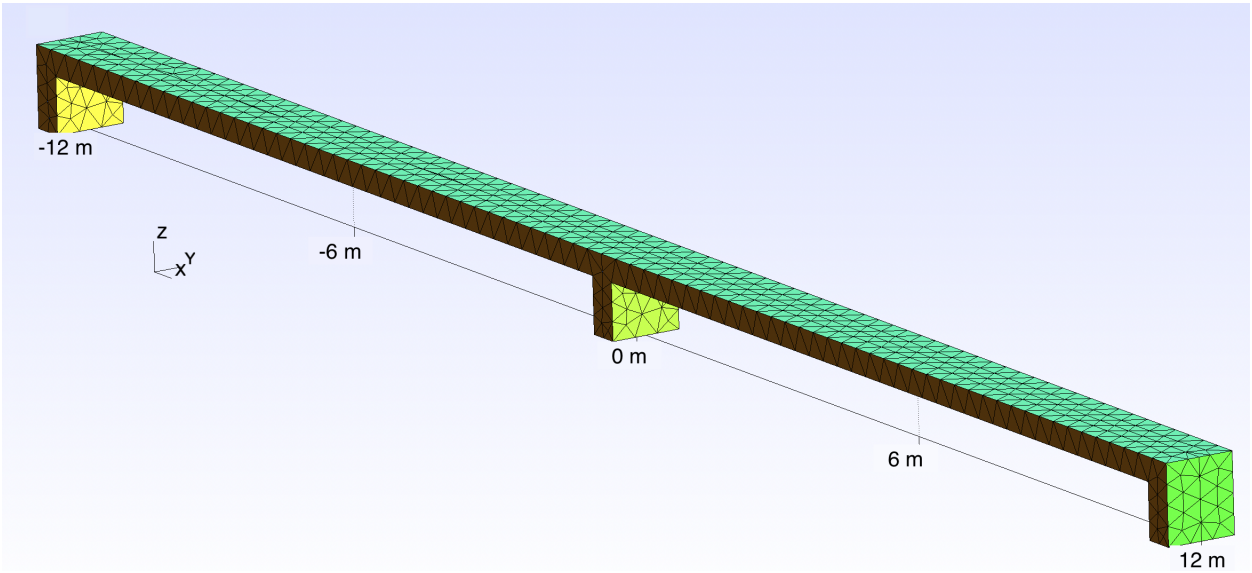

Figure 5: Tetrahedral mesh of the bridge generated by Gmsh. It has the same dimensions as the real bridge model.

with a radius of approximately 0.3 m. We then compare the measured dv/v values of all 6C receivers.

Table 1: Elastic parameters of the numerical bridge model.

Density	Young's modulus	Poisson ratio
2300 kg/m^3	33000 Mpa	0.2

For the first set of numerical experiments, the point source and the 6C receiver are positioned along the same span of the model, replicating the aperture configuration of the actual experiment. In Figure 7a, the modeled vertical component of acceleration and horizontal component of rotational rate are displayed before and after applying a band-pass filter. The proposed 6C method is then applied to the filtered data, with Figure 7b presenting the measured dv/v as a function of the theoretical reduction of Young's modulus. The observed changes in dv/v are proportional to those of Young's modulus, as anticipated. These numerical results validate the achieved dv/v due to external load and prestress loss during the real experiment.

For the second set of numerical experiments, the location of the embedded damage zone is indicated by the red circle in Figure 8a. The localized damage zone is characterized by a reduction in Young's modulus. With a total of 21 6C receivers spaced at 2 m intervals, the source position remains consistent with that of the first experiment. The same data processing is applied to each 6C receiver, and their respective dv/v values before and after embedding the damage zone are depicted in Figure 8b, with the dashed red line marking the position of the damage zone. It is evident that the 6C receiver closest to the damage zone exhibits the most pronounced dv/v. These results confirm the near-receiver sensitivity of the 6C method, showcasing its ability to more accurately locate potential small damages compared to

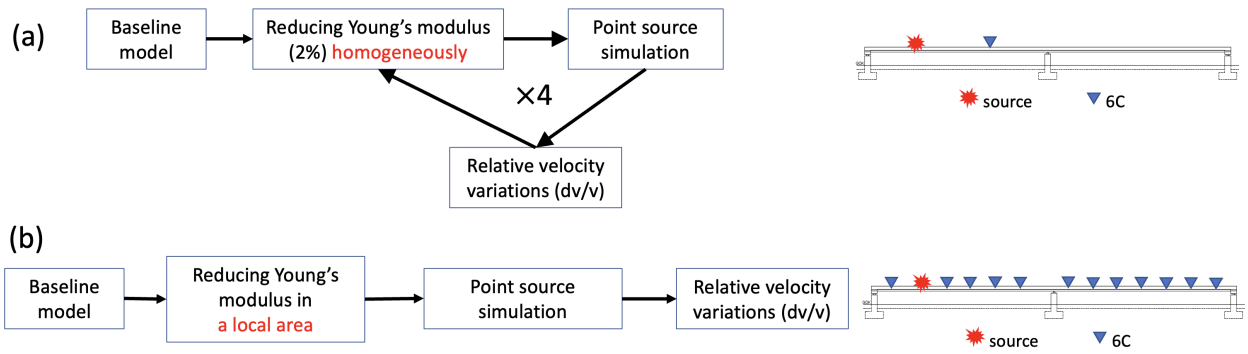

Figure 6: Two sets of numerical simulations and analyses to validate the proposed 6C amplitude ratio method. (a) Starting from a baseline model, we gradually reduce Young's modulus uniformly across the bridge model. (b) Using a series of 6C receivers and a single source, we introduce a low-velocity zone to simulate a damage zone.

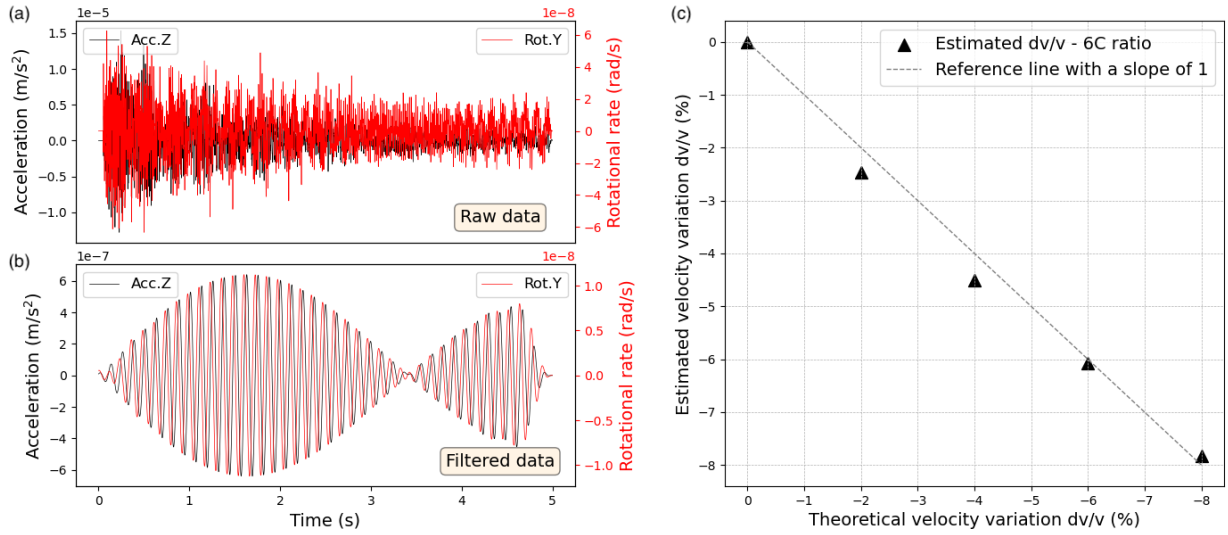

Figure 7: The estimated dv/v using the 6C method for the bridge with different Young's moduli. (a) and (b) The raw and filtered acceleration and rotational rate recordings. (c) The estimated dv/v compared to the theoretical dv/v.

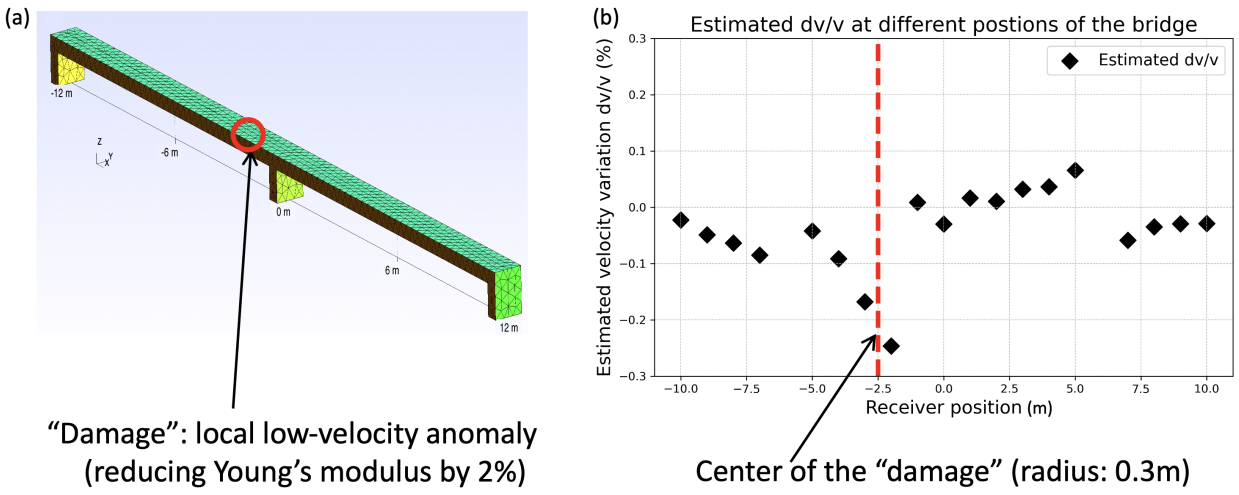

Figure 8: The results of the simulation where we add local damage zone. (a) Schematic illustration of the bridge model and the location of the damage zone indicated by the red circle. (b) The estimated dv/v based on the 6C amplitude ratio method for each receiver along the bridge. The dashed red line indicates the location of the added damage zone.

conventional methods.

5 Discussion and conclusions

In this paper, we propose a novel single-station 6C measurement for bridge structural health monitoring. Both real and synthetic experiments demonstrate that the joint analysis of translational and rotational data can effectively identify damage and quantify structural variations. The results are consistent with those obtained from coda wave interferometry using ultrasonic recording, as shown by Liao et al. (2021). By simulating 3D wave propagation and analyzing the spatial gradient of the wavefield in a concrete beam, we validate the developed 6C amplitude ratio method. This amplitude-ratio approach offers near-receiver sensitivity, which aids in damage localization while mitigating environmental and source effects, making 6C measurements robust and reliable for bridge health monitoring.

In our second set of numerical examples featuring a single local damage zone, we notice that the estimated dv/v value (-0.25%) from the 6C receiver closest to the damage zone is significantly smaller than the true reduction in Young's modulus (-2%). This discrepancy might be attributed to two main factors. First, despite the near-receiver sensitivity of the 6C method, the measured dv/v still represents an average velocity change over a certain spatial range. The localized nature of the low-velocity anomaly means its effect is diluted by the larger volume of unchanged medium surrounding it, resulting in a smaller overall dv/v measurement. Second, our focus on fundamental mode vibrations may influence how the local anomaly is sampled. The sensitivity of both translational and rotational vibrations to the anomaly can vary based on the frequency content, potentially leading to an underestimation of the true velocity change.

In real damage scenarios, the reduction in Young's modulus for a bridge is likely to exceed 2%. However, the chosen value of 2% for the noise-free synthetic validation should not affect the overall conclusions.

Although this study focused on fundamental mode vibrations, the proposed amplitude-ratio method is applicable to higher modes as well. While the estimated relative velocity variations may differ from those of the fundamental mode, the overall trend of structural changes and damage implications is expected to remain consistent. Future research could explore the comparative spatial resolution for damage identification and localization using different vibration modes.

Our narrow bridge model and weight-drop source are designed to primarily generate two-dimensional vibrations, allowing us to simplify the analysis by focusing on rocking vibrations. However, in real–world scenarios, larger bridges–with their more complex structures and varied vibration patterns—will require a more comprehensive analysis that includes all components of translational and rotational motion when calculating amplitude ratios. We could extend the 6C method to account for torsional vibrations by analyzing horizontal translational motions alongside vertical rotational motions. By integrating the dv/v estimates from both rocking and torsional modes, we can provide a more robust quantification of structural variations in bridges, enhancing our ability to detect and characterize different types of structural changes or damage.

The data analysis required for the proposed method is suitable for real-time monitoring with limited computing resources, as it involves a simple comparison of a previously calculated amplitude ratio to the current one. The most computationally demanding step in calculating the current amplitude ratio is the Hilbert transform of time series data as they are acquired, but this can be done in real time (Prince et al., 2015).

Data and resources

Data and models that support the findings of this study are available from the corresponding author upon request.

Acknowledgments

The authors would like to extend their gratitude to Dr. Falk Hille and his team from BAM division 7.2, Joachim Bülow and Regina Maaß from University of Hamburg and Saskia Steibel from Ludwig-Maximilians-Universität München for their support during the field experiment. This study is part of the GIOTTO project (Grant No. 03G0885A), funded by Bundesministerium für Bildung und Forschung (BMBF). This research is also supported by the European Research Council (ROMY project, Grant No. 339991), the National Science Foundation (Award No. 2046387), and the U.S. Geological Survey Earthquake Hazards Program (Grant No. G24AS00292).

References

Alamdari, M. M., Kildashti, K., Samali, B., and Goudarzi, H. V. (2019). Damage diagnosis in bridge structures using rotation influence line: Validation on a cable-stayed bridge. *Engineering Structures*, 185:1–14.

Alten, K., Ralbovsky, M., Vorwagner, A., Toplitzer, H., and Wittmann, S. (2017). Evaluation of different monitoring techniques during damage infliction on structures. *Procedia Engineering*, 199:1840–1845.

Barak, O., Key, K., Constable, S., and Ronen, S. (2018). Recording active-seismic ground rotations using induction-coil magnetometers. *Geophysics*, 83(5):P19–P42.

Bernauer, F., Garcia, R. F., Murdoch, N., Dehant, V., Sollberger, D., Schmelzbach, C., Stähler, S., Wassermann, J., Igel, H., Cadu, A., et al. (2020a). Exploring planets and asteroids with 6DoF sensors: Utopia and realism. *Earth, Planets and Space*, 72:1–18.

Bernauer, F., Wassermann, J., and Igel, H. (2020b). Dynamic tilt correction using direct rotational motion measurements. *Seismological Society of America*, 91(5):2872–2880.

Bernauer, M., Fichtner, A., and Igel, H. (2009). Inferring earth structure from combined measurements of rotational and translational ground motions. *Geophysics*, 74(6):WCD41–WCD47.

Donner, S., Bernauer, M., and Igel, H. (2016). Inversion for seismic moment tensors combining translational and rotational ground motions. *Geophysical Journal International*, 207(1):562–570.

Dumbser, M. and Käser, M. (2006). An arbitrary high-order discontinuous Galerkin method for elastic waves on unstructured meshes—ii. the three-dimensional isotropic case. *Geophysical Journal International*, 167(1):319–336.

Heng, Z., Shu-Ying, Q., and Guo-Liang, W. (2014). Research on the method of simply supported beam modal parameters recognition by qy iinclinometer. *Journal of Applied Sciences*, 14(16):1844–1850.

Hester, D., Brownjohn, J., Huseynov, F., Obrien, E., Gonzalez, A., and Casero, M. (2020). Identifying damage in a bridge by analysing rotation response to a moving load. *Structure and Infrastructure Engineering*, 16(7):1050–1065.

Huseynov, F., Kim, C., Obrien, E. J., Brownjohn, J., Hester, D., and Chang, K. (2020). Bridge damage detection using rotation measurements–experimental validation. *Mechanical Systems and Signal Processing*, 135:106380.

InfrastructureCard (2021). 2021 infrastructure report.

Keil, S., Wassermann, J., and Igel, H. (2021). Single-station seismic microzonation using 6C measurements. *Journal of Seismology*, 25:103–114.

Lee, W. H., Igel, H., and Trifunac, M. D. (2009). Recent advances in rotational seismology. *Seismological Research Letters*, 80(3):479–490.

Liao, C.-M., Hille, F., Barroso, D. F., and Niederleithinger, E. (2021). Monitoring of a prestressed bridge model by ultrasonic measurement and vibration recordings. In *COMPDYN 2021 8th ECCOMAS Thematic Conference on Computational Methods in Structural Dynamics and Earthquake Engineering*, pages 1–9. European Community on Computational Methods in Applied Sciences (ECCOMAS).

Limongelli, M. P. and Çelebi, M. (2019). *Seismic structural health monitoring: from theory to successful applications*. Springer.

Lin, C.-J., Huang, H.-P., Liu, C.-C., and Chiu, H.-C. (2010). Application of rotational sensors to correcting rotation-induced effects on accelerometers. *Bulletin of the Seismological Society of America*, 100(2):585–597.

McGeown, C., Huseynov, F., Hester, D., McGetrick, P., Obrien, E., and Pakrashi, V. (2021). Using measured rotation on a beam to detect changes in its structural condition. *Journal of Structural Integrity and Maintenance*, 6(3):159–166.

Obrien, E. J., Brownjohn, J., Hester, D., Huseynov, F., and Casero, M. (2021). Identifying damage on a bridge using rotation-based bridge weigh-in-motion. *Journal of Civil Structural Health Monitoring*, 11:175–188.

Pakrashi, V., Harkin, J., Kelly, J., Farrell, A., and Nanukuttan, S. (2013). Monitoring and repair of an impact damaged prestressed bridge. In *Proceedings of the Institution of Civil Engineers-Bridge Engineering*, volume 166, pages 16–29. Thomas Telford Ltd.

Prince, A. A., Verma, P. K., Jayakumar, C., and Raju, D. (2015). Efficient architecture for real time implementation of hilbert transform in fpga. In *2015 IEEE International Conference on Electrical, Computer and Communication Technologies (ICECCT)*, pages 1–5. IEEE.

Rossi, Y., Tatsis, K., Hohensinn, R., Clinton, J., Chatzi, E., and Rothacher, M. (2024). Unscented kalman filter–based fusion of gnss, accelerometer, and rotation sensors for motion tracking. *Journal of Structural Engineering*, 150(7):05024002.

Sollberger, D., Igel, H., Schmelzbach, C., Edme, P., Van Manen, D.-J., Bernauer, F., Yuan, S., Wassermann, J., Schreiber, U., and Robertsson, J. O. (2020). Seismological processing of six degree-of-freedom ground-motion data. *Sensors*, 20(23):6904.

Wang, H., Igel, H., Gallovič, F., and Cochard, A. (2009). Source and basin effects on rotational ground motions: Comparison with translations. *Bulletin of the Seismological Society of America*, 99(2B):1162–1173.

Yuan, S., Gessele, K., Gabriel, A.-A., May, D. A., Wassermann, J., and Igel, H. (2021). Seismic source tracking with six degree-of-freedom ground motion observations. *Journal of Geophysical Research: Solid Earth*, 126(3):e2020JB021112.

Yuan, S., Simonelli, A., Lin, C.-J., Bernauer, F., Donner, S., Braun, T., Wassermann, J., and Igel, H. (2020). Six degree-of-freedom broadband ground-motion observations with portable sensors: Validation, local earthquakes, and signal processing. *Bulletin of the Seismological Society of America*, 110(3):953–969.

Zembaty, Z., Kokot, S., and Bobra, P. (2014). Application of rotation rate sensors in structural health monitoring. In *Proceedings of the 9th International Conference on Structural Dynamics, EURODYN 2014*.